

MECHANICAL ALIGNMENT OF SUPRATHERMAL PARAMAGNETIC COSMIC-DUST GRANULES: THE CROSS SECTION MECHANISM

MICHAEL EFROIMSKY

Institute for Mathematics and Its Applications, University of Minnesota, 207 Church Street SE, Suite 400, Minneapolis, MN 55455
 Received 2002 February 11; accepted 2002 April 25

ABSTRACT

We develop a comprehensive quantitative description of the cross section mechanism discovered by Lazarian. This is one of the processes that determine grain orientation in clouds of suprathermal cosmic dust. The mechanism manifests itself when an ensemble of suprathermal paramagnetic granules is placed in a magnetic field and is subject to ultrasonic gas bombardment. The mechanism yields dust alignment whose efficiency depends on two factors: the geometric shape of the granules and the angle Φ between the magnetic line and the gas flow. We calculate the quantitative measure of this alignment and study its dependence on the said factors. It turns out that, irrelevant of the grain shape, the action of a flux does not lead to alignment if $\Phi = \arccos(1/\sqrt{3})$.

Subject heading: dust, extinction

1. INTRODUCTION: THE PHYSICAL NATURE OF EFFECT

Starlight polarization is a long-known effect. Because of its correlation with reddening, the phenomenon is explained by alignment of particles in dust nebulae (Hall 1949; Hiltner 1949). The alignment causes differential extinction of electromagnetic waves of different polarizations and provides a remarkable example of order emerging in a seemingly chaotic system.

In a nutshell, the polarization is due to the grains' nonsphericity. A grain has different cross sections, and these are somehow aligned within the cloud. A remarkable fact is that, whatever orientational mechanisms show themselves in the grain dynamics, the alignment always takes place relative to the interstellar magnetic field.

Rotational dynamics of an interstellar particle is determined by a whole bunch of accompanying physical processes whose combination produces a variety of orientational mechanisms. Which of these come into play in a particular physical setting depends on the suprathermality of the dust cloud. Suprathermal grains are, by definition, grains that spin so rapidly that their averaged (over the dust ensemble) rotational kinetic energy $\langle E_{\text{rot}} \rangle$ much exceeds the (multiplied by the Boltzmann constant κ) temperature T_{gas} of the surrounding environment. The suprathermality degree is then introduced as the following ratio:

$$\beta = \frac{\langle E_{\text{rot}} \rangle}{\kappa T_{\text{gas}}} . \quad (1)$$

Dust ensembles with β of order unity are called thermal or Brownian. Clouds with $\beta \gg 1$ are called suprathermal. In the observable universe, values of β of order 10^2 are not unusual.

The leading reason for suprathermal rotation is formation of H_2 molecules at the defects on the granule surface: over such a defect (called active site), two atoms of H couple to form a molecule, ejection whereof applies an uncompensated torque to the granule surface (Purcell 1979). These so-called spin-up torques keep emerging at each active site until the site gets “poisoned” through the everlasting accretion. After that, some other active site will dominate the spin

dynamics of the grain, by its H_2 “rocket.” This change of spin state will, with some probability, go through a short-term decrease, to thermal values, of the grain's angular velocity. Such breaks are called “crossovers” or “flip-overs.”

Another pivotal issue is the existing evidence of paramagnetic nature of a considerable share of dust particles (Whittet 1992) that makes them subject to the Barnett effect. The latter takes place in para- and ferromagnetics because of interaction between the spins of unpaired electrons and the macroscopic rotation of crystal lattice (Stoner 1934). The coupling has its origin in the angle-dependent terms in the dipole-dipole interaction of neighboring spins. It spontaneously endows a rotating para- or ferromagnetic body with a magnetic moment parallel to the angular velocity¹ (Lazarian & Roberge 1997). Purcell offered the following illustration. If a rotating body contains an equal amount of spin-up and spin-down unpaired electrons, its magnetization is nil. Its kinetic energy would decrease, with the total angular momentum remaining unaltered, if some share of the entire angular momentum could be transferred to the spins by turning some of the unpaired spins over (and, thus, by dissipating some energy). This potential possibility is brought to pass through the said coupling.

An immediate outcome from granule magnetization is the subsequent coupling of the magnetic moment \mathbf{M} with the interstellar magnetic field \mathbf{B} —the magnetic moment precesses about the magnetic line. What is important is that this precession takes place at an intermediate rate. On the one hand, it is slower than the grain's spin about its instantaneous rotation axis. On the other hand, the precession period is much shorter than the typical timescale at which the relative-to- \mathbf{B} alignment gets established.² The latter was proven by Dolginov & Mytrofanov (1976) for magnetization resulting from the Barnett effect and by Martin (1971) for magnetization resulting from the grain's charge.

¹ Another contribution to the magnetization comes from the electric charge carried by the granule.

² A more exact statement, to be needed below, is that the period of precession (about \mathbf{B}) of the magnetic moment \mathbf{M} (and of the major-inertia axis Z aligned therewith) is much shorter than the mean time between two sequent flip-overs of a spinning granule (Purcell 1979; Roberge, DeGraff, & Flaherty 1993).

If we disembodify the core idea of the Barnett effect from its particular implementation, we shall see that it is of quite a general sort: a free top, although conserving its angular momentum, tends to minimize its kinetic energy through some dissipation mechanism(s). This fact, omitted in the Euler-Jacobi theory of unsupported top, makes their theory inapplicable at timescales comparable to the typical time of dissipation (Efroimsky 2002). The needed generalization of the unsupported-top dynamics constitutes a mathematically involved area of study (Efroimsky 2000), which provides ramifications for wobbling asteroids and comets (Efroimsky 2001), rotating spacecraft, and precessing pulsars (Trümper et al. 1986; Alpar & Ögelman 1987; Bisnovatyi-Kogan & Kahabka 1993; Stairs et al. 2000). Fortunately, in the case of cosmic-dust physics, we need only some basics of this theory. A free rotator has its kinetic energy minimized (with its angular momentum being fixed) when the rotation axis coincides with the axis of major inertia. In this so-called principal state, the major-inertia axis Z , the angular velocity Ω , and the angular momentum vector \mathbf{J} are all aligned. In other, complex rotation states, both the maximal-inertia axis Z and angular velocity Ω precess about the angular momentum \mathbf{J} . This precession is also called “wobble” or “tumbling,” in order to distinguish it from the precession of the magnetic moment \mathbf{M} about the magnetic line. Similarly, the wobble relaxation (i.e., gradual alignment of axis Z and of Ω toward \mathbf{J}) should be distinguished from the granule alignment relative to the magnetic field \mathbf{B} : the latter effect is the eventual target of our treatise, while the former is merely a thread in the tapestry. Still, the wobble relaxation is far more than a mere technicality: it is important to know if a typical time of the wobble relaxation is much less than the typical times of the external interactions (like, say, the period of precession of \mathbf{M} about \mathbf{B}). In case the wobble relaxation is that swift, one may assume that the precession (about \mathbf{B}) of the magnetic moment \mathbf{M} is the same as precession of the angular momentum \mathbf{J} about \mathbf{B} ; indeed, in this case, both \mathbf{J} and the major-inertia axis Z will be aligned with Ω , which is parallel to \mathbf{M} . This parallelism of all four vectors is often called not alignment but “coupling,” to distinguish it from the alignment relative to \mathbf{B} . This coupling is enforced by two different processes. One is an effect kin to that of Barnett: tumbling of Ω relative to conserved³ \mathbf{J} (and, therefore, relative to an inertial observer) yields periodic remagnetization of the material, which results in dissipation. The other effect is the anelastic dissipation: in a complex rotational state the points inside the body experience time-dependent acceleration that produces alternate stresses and strains. Anelastic phenomena entail inner friction (which may be understood also in terms of a time lag between the strain and stress). The contributions from the Barnett and anelastic effects to the coupling were compared by Purcell in his long-standing cornerstone work (Purcell 1979). Purcell came to an unexpected conclusion that the input from the Barnett effect much outweighs that from anelasticity. An accurate treatment (Lazarian & Efroimsky 1999) shows that the anelastic dissipation is several orders of magnitude more effective than presumed, and in many physical settings it dominates over the Barnett dissipation. The case of suprathermal dust is one such setting. Without going into redundant details, we would mention that combination of the two

³ The angular momentum is conserved at timescales shorter than the duration of a precession cycle of \mathbf{J} about \mathbf{B} .

dissipation processes provides at least partial alignment of Z and Ω toward \mathbf{J} in Brownian clouds, and it provides a perfect alignment in suprathermal ones.

The presently known mechanisms of grain alignment can be classified into three categories: mechanical mechanisms, paramagnetic mechanisms, and via radiative torques. The latter mechanism was addressed in Dolginov & Mytrofanov (1976), Lazarian (1995a), and Draine & Weingartner (1996, 1997). It has not yet been well understood. The paramagnetic alignment is due to the Davis-Greenstein (1951) mechanism (initially suggested for Brownian dust particles) and to the Purcell (1979) mechanism (which is a generalization of the Davis-Greenstein mechanism to the suprathermal case). The Davis-Greenstein and Purcell processes operate to bring the granule’s rotation axis (which is, as explained above, fully or partially aligned with the granule’s major-inertia axis) into parallelism with the magnetic line. This happens because precession of the grain’s spin axis about \mathbf{B} entails material remagnetization⁴ and, therefore, dissipation resulting in a slow removal of the rotation component orthogonal to \mathbf{B} . The induced alternating magnetization \mathbf{M} will lag behind rotating \mathbf{B} , giving birth to a nonzero torque equal, in the body frame, to $\mathbf{M} \times \mathbf{B}$. It can be shown (Davis & Greenstein 1951) that this torque will entail steady decrease of the orthogonal-to- \mathbf{B} component of the angular velocity.⁵ The so-called⁶ mechanical alignment comprises the Gold (1952) mechanism and those of Lazarian (1995a, 1995b, 1995c, 1995d, 1995e). Lazarian suggested two mechanisms, the crossover one and the cross section one, and they show themselves in the case of suprathermal grains only.

The nature of the Gold mechanism is the following. Each collision of the dust particle with an atom or a molecule of the streaming gas adds to the particle’s angular momentum a portion perpendicular to the relative velocity. As explained above, the major-inertia axis of the body tends to align with the angular momentum vector. One, hence, may say that the interstellar wind will spin up the granule so that its maximal-inertia axis will “prefer” positions perpendicular to the wind. Since the said major-inertia axis is, roughly, the shortest dimension of the rotator, one may deduce that, statistically, the particles tend to rotate with their shortest axes orthogonal to the gas flow. This picture is, however, complicated by the precession of the magnetic moments (and of the angular momenta that tend, for the aforementioned reason, to align with the magnetic moments) about the magnetic line. This mechanism works only for Brownian dust clouds because it comes into being as a result of the elastic gas-grain collisions to which only thermal granules are sensitive. To be more exact, it is assumed here that the precession period is much shorter than a typical time during which the grain’s angular momentum alters considerably.

The suprathermally rotating dust particles ignore the random torques caused by the elastic gas-grain collisions

⁴ It is assumed that the grain is either paramagnetic (Davis & Greenstein 1951) or ferromagnetic (Spitzer & Tukey 1951; Jones & Spitzer 1967). The case of a diamagnetic granule has not been addressed in the literature so far.

⁵ A rigorous analysis of the Davis-Greenstein process should be carried out in the language of the Fokker-Planck equation (Jones & Spitzer 1967).

⁶ The word “so-called” is very much in order here because the mechanical mechanisms, too, provide alignment relative to the magnetic line. Their name “mechanical” simply reflects the fact that these effects are not purely magnetic but involve the grains’ mechanical interaction with the gas flow.

because the timescales for the random torques to alter the spin state are several orders of magnitude larger than the average time between subsequent crossovers (Purcell 1979). Still, the dust granules do become susceptible to the random torques during the brief crossovers when the granule becomes, for a short time, thermal (i.e., slow spinning). This is the essence of the first Lazarian mechanism of alignment, introduced in Lazarian (1995b) under the name of “cross-over mechanism.” Hence, the first Lazarian mechanism is the Gold alignment generalized for suprathermal grains, the generalization being possible because even suprathermal granules become thermal for small time intervals.

The second Lazarian mechanism, termed “cross section mechanism” by Lazarian (1995b, 1995e) and studied in Lazarian & Efroimsky (1996) and Lazarian, Efroimsky, & Ozik (1996), is not a generalization of any previously known effect but is a totally independent, very subtle phenomenon. The underlying physical idea is simple: a precessing (about the magnetic line) interstellar granule will “prefer” to spend more time in a rotational mode of the minimal effective cross section. In other words, the particle has to “find” the preferable mean value of its precession cone’s half-angle, a value that will minimize the mean cross section. Here the “mean cross section” is the averaged (over rotation, and then over precession) cross section of a granule as seen by an observer looking along the direction of interstellar drift. It is crucial that, although the alignment is due to gas-grain collisions, it establishes not relative to the wind direction but relative to the magnetic line about which the spinning grain is precessing.

Now, the goal is to know how effective this mechanism is for dust particles of various shapes. In Lazarian & Efroimsky (1996) and Lazarian et al. (1996) we addressed the cross section alignment of oblate and prolate symmetrical grains. In the current paper we intend to extend the study to ellipsoidal granules of arbitrary ratios between the semiaxes.

2. STARLIGHT EXTINCTION ON INTERSTELLAR DUST

Starlight attenuation by dust, called extinction, comprises two separate phenomena: scattering and absorption. The final result is a cooperative effect of all particles the ray bypasses.

Absorption is taking place on different grains independently from one another. For scattering such independence is not, generally, guaranteed. Still, in our study we deal solely with the independent scattering and omit the phase relations between waves scattered by neighboring grains. This is justified by the starlight not being monochromatic: the lack of coherence in it excludes any phase-related phenomena.⁷ Thence, the intensities of waves scattered from various granules must be added without regard to phase. Finally, we shall be blithe about the multiple scattering because it has almost no effect on the attenuation process. Indeed, the granules are separated by distances exceeding their size by many orders of magnitude, and the optical depth of most interstellar⁸ dust clouds is well below unity.

⁷ In the future, it may be good to measure the starlight polarization at separate wavelengths.

⁸ This is not necessarily true for circumstellar environments where the dust is more abundant.

The starlight-scattering differential cross section on a dust grain is introduced, in a pretty standard manner, as the incident wave front area wherefrom the photons get scattered into solid angle $d\Omega$, divided by this solid angle: $dC_{\text{scat}}/d\Omega$. Its integral over $d\Omega$ would then give the full cross section C_{scat} of the process. However, it would be physically incomplete to interpret C_{scat} simply as the incident wave front area whence the photons get scattered off their initial direction. As well known since the times of Newton and Huygens, the corpuscular interpretation neglects the interference of the scattered and incident components of light. Therefore, it will fail to describe the forward scattering. The problem is somewhat subtle. On the one hand, the mathematical expression for differential cross section formally remains correct for any finite value of the scattering angle θ . Indeed, for an arbitrarily small but finite angle, the observer potentially *can* distinguish between the primary and the scattered images. To that end, he will have to employ a sufficiently powerful telescope located at a sufficiently remote distance from the scatterer. On the other hand, the needed resolving power of the telescope must be achieved by increasing the size of the object lens. The finite radius of lenses thereby imposes a restriction on the scattering angle values.⁹ Hence, the expression for full cross section C_{scat} is of no physical interest. It corresponds to no physical measurement because it is pointless to carry out the integration over too close a vicinity of $\theta = 0$. Starlight extinction on the cosmic dust is such a case: with the distances grossly exceeding the device size, the observations are performed at effectively zero scattering angles, so the telescope does not distinguish the forward-scattered light from the primary wave. A simple estimate (van de Hulst 1957) that takes into account the interference leads to the natural conclusion that in the forward-scattering case the scatterer reduces the light energy entering the telescope. This relative reduction is called *forward-scattering cross section*:

$$C_{\text{fs}}(\omega) = \frac{4\pi}{k^2} \text{Re}\{S(0)\}, \quad (2)$$

$S(0)$ being the amplitude of the incident beam, in the direction from the source toward the observer. Roughly speaking, the observer will get an impression that a certain share C_{fs}/A of the object lens area A is covered up. This shows the fundamental difference between the scattering cross section and forward-scattering cross section: while the former is associated with the area of the incident wave front, the latter is associated with that of the observer’s aperture. This profound difference stems from our inability to separate the front-scattered light from the incident wave. As agreed above, we consider only optically thin clouds. This means that we totally ignore C_{scat} but do take C_{fs} into account.

Physically, it is quite obvious that absorption will come into play through adding some C_{abs} to C_{fs} . Even less light will reach the lens, and the observed intensity will be

$$I_0(\omega)[A - C_{\text{fs}}(\omega) - C_{\text{abs}}(\omega)]. \quad (3)$$

⁹ Suppose that our telescope is aimed at a distant star, the scatterer being slightly off the line of sight. In order for the secondary image to get into the object lens, the scattered photons must be deflected at angles not exceeding R/r , with R and r being the radius of the lens and the distance to the scatterer, respectively. At the same time, the angular resolution of the lens is less than λ/R . This results in the trivial inequality $\lambda/R < R/r$, whence $R > (\lambda r)^{1/2}$.

In the end of the preceding section we agreed that the light extinction by different granules is independent and is free from phase correlations: the intensity losses simply add. This will result in the extinction cross sections of the single granules added to give the extinction cross section of the entire cloud (for a detailed explanation see van de Hulst 1957, pp. 31–32). Finally, for whatever real observation, the above expression must be multiplied by the window function $W(\omega)$ of the device and integrated over ω . All in all, the resulting attenuation will be expressed by the extinction cross section

$$C_{\text{ext}} = \frac{\int_0^\infty W(\omega) I_0(\omega) \sum_i \left[C_{\text{fs}}^{\{i\}}(\omega) + C_{\text{abs}}^{\{i\}}(\omega) \right] d\omega}{\int_0^\infty W(\omega) I_0(\omega) d\omega}, \quad (4)$$

where i is the number of a particle and $C_{\text{abs,fs}}^{\{i\}}$ is its cross section. If $W(\omega)$ carves out a band wherein $C_{\text{fs}}^{\{i\}} + C_{\text{abs}}^{\{i\}}$ depends on ω weakly, we are left with

$$C_{\text{ext}} \approx \sum_i (C_{\text{fs}}^{\{i\}} + C_{\text{abs}}^{\{i\}}). \quad (5)$$

All of the above is valid for both polarizations independently. Thus, the scattering, forward-scattering, absorption, and extinction cross sections may be introduced for them separately.

3. THE MEASURE OF ALIGNMENT: ITS RELATION TO POLARIZATION

In § 1 we explained what it means for an interstellar grain to be aligned. For the effect to be quantified, it should be endowed with some reasonable measure, one that would interconnect the dust dynamics with the starlight polarization degree.

Linear polarization essentially means that if the ray propagates in the z_o -direction, there exist two (orthogonal to z_o and to one another) directions, x_o and y_o , appropriate to the maximal and minimal magnitudes of the electric field in this ray. The subscript “ o ” signifies the observer’s frame. The question now is, how will these maximal and minimal magnitudes E_x^o and E_y^o (or, equivalently, the maximal and minimal intensities E_x^{o2} and E_y^{o2}) evolve along the line of sight, within the cloud? Properly speaking, one should talk about the ensemble averages of these intensities, $\langle E_x^{o2} \rangle$ and $\langle E_y^{o2} \rangle$, the averaging being implied first over the grain orientation (relative to its angular momentum), then over the angular momentum’s precession about the magnetic field, and finally over the half-angle β of the precession cone. (The direction of magnetic field will be assumed to be constant over the line of sight, within the cloud.) While each of the first two averagings will be merely an integration over a full circle, the latter averaging will involve some distribution function for β . This distribution function should be provided by the detailed theory of a particular orientational mechanism dominating the alignment process.

In neglect of the secondary scattering, the decrease in intensity dI is proportional to the length dz and to the dust particle density n in the cloud: $dI = -C_{\text{ext}} n dz$, with C_{ext} being the aforementioned extinction cross section (eq. [4]). What we observe are the intensities at the exit from the nebula. Call them $\langle E_x^{o2} \rangle$ and $\langle E_y^{o2} \rangle$. Then

$$\langle E_x^{o2} \rangle \sim \exp(-C_x^o n l), \quad \langle E_y^{o2} \rangle \sim \exp(-C_y^o n l), \quad (6)$$

l being the depth of the cloud as seen by the observer and $C_{x,y}^o$ being the mean extinction cross sections for the two linear polarizations orthogonal to the observer’s line of sight.

Suppose that, prior to entering the nebula, the starlight was unpolarized. One can characterize the polarizing ability of the cloud by the measured flux intensity I as a function of the angle of rotation of some analyzing element of the telescope. In practice, they rather employ a relative measure, P_{ext} , which is the degree of polarization due to selective extinction:

$$P_{\text{ext}} \equiv \frac{I_x - I_y}{I_x + I_y} = \frac{\langle E_x^{o2} \rangle - \langle E_y^{o2} \rangle}{\langle E_x^{o2} \rangle + \langle E_y^{o2} \rangle}. \quad (7)$$

As follows from the above formulae,

$$P_{\text{ext}} = \frac{\exp(-C_x^o n l) - \exp(-C_y^o n l)}{\exp(-C_x^o n l) + \exp(-C_y^o n l)} \approx \frac{C_x^o n l - C_y^o n l}{2},$$

the approximation being valid for $P_{\text{ext}} \ll 1$ (with no need to assume that $C^o n l \ll 1$). The measure of polarization involves the difference ($C_x^o - C_y^o$) that depends on the extinction properties of a single grain and on the degree of alignment in the cloud. The topic was addressed by many. A brief conclusion that saves type will be as follows: no matter which alignment mechanism dominates, the difference ($C_x^o - C_y^o$) should be expressed as a function of a single granule’s extinction cross sections and of the magnetic field direction (relative to the line of sight). Naturally, the said difference will also be a functional of the precession cone half-angle distribution. This half-angle, often denoted as β , comprises the angular separation between the magnetic field and the particle’s angular momentum precessing thereabout. The statistical distribution of β over the ensemble depends on the dominating orientational mechanism(s), and its calculation is a technical issue that sometimes is extremely laborious.

Expressions for $C_{x,y}^o$ in terms of the aforementioned arguments are given, for oblate and prolate symmetrical granules, in Greenberg (1968), Purcell & Spitzer (1971), Lee & Draine (1985), Hildebrand (1988), and Roberge & Lazarian (1999). To fulfil the goal of our study, we must generalize those results for the case of triaxial ellipsoid. To this end, we introduce the extinction cross sections $C_{X,Y,Z}$ of the grain, for light polarized along its minimal- (X), middle- (Y), and maximal-inertia (Z) axes.¹⁰ Calculation, presented in Appendix A, results in the relation

$$C_x^o - C_y^o = \left(\frac{C_X + C_Y}{2} - C_Z \right) R \cos^2 \gamma, \quad (8)$$

where γ is the angle between the magnetic field and the plane of sky (Fig. 1) and R is the so-called Rayleigh reduction factor defined as

$$R \equiv \frac{3}{2} \left(\langle \cos^2 \beta \rangle - \frac{1}{3} \right), \quad (9)$$

β being the half-angle of the precession cone described by the grain’s angular momentum about the magnetic line (Fig. 2). As already mentioned, this angle is not the same for

¹⁰ These cross sections characterize particular species of dust. Computation of these is comprehensively discussed by van de Hulst (1957; see also Martin 1974; Draine & Lee 1984).

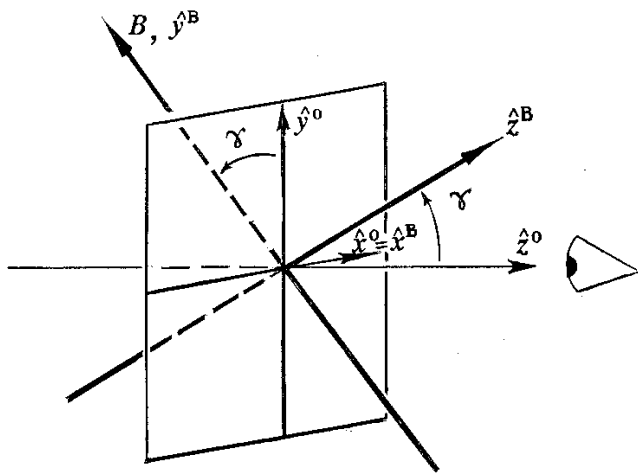


FIG. 1.—Line of sight, plane of sky, and direction of magnetic field. Axes y^0 and z^0 are chosen to belong to the plane defined by the line of sight and magnetic line.

all grains but obeys some statistical distribution determined by a particular physical setting. The above formula for R was obtained assuming principal rotation (when the alignment of the principal axis with the angular momentum is promptly enforced), valid for suprathermally rotating grains (Lazarian & Efroimsky 1999). In the thermal case, when angle θ between the angular momentum and the major-inertia axis is nonzero, the Rayleigh factor would look more complicated:

$$R = \left\langle \frac{3}{2} (\cos^2 \beta - \frac{1}{3}) \frac{3}{2} (\cos^2 \theta - \frac{1}{3}) \right\rangle. \quad (10)$$

Returning to equation (9), we would point out the evident fact that in the absence of alignment, the ensemble average

of $\cos^2 \beta$ is equivalent to averaging simply over the solid angle: $\langle \cos^2 \beta \rangle = \frac{1}{3}$. This nullifies the R factor and makes the radiation unpolarized: $C_x^o = C_y^o$.

4. CALCULATION OF THE RAYLEIGH REDUCTION FACTOR

The basic idea of the cross section orientational process (pioneered by Lazarian 1995b, 1995e) comes from the fact that the average time between two sequent crossovers is proportional to a typical lifetime of an active site (“Purcell rocket”). Each such site is eventually “poisoned” through the evergoing accretion of atoms brought by the interstellar wind. Emergence of new active sites leads to crossovers. Henceforth, the higher the accretion rate, the shorter the average lifetime of a typical Purcell rocket. Now, since the atoms adsorbed by the surface get delivered through the gas bombardment, one may state that the said lifetime is proportional to the rate of gas-grain collisions. The latter rate, in its turn, is proportional to the gas-grain effective cross section, i.e., to the averaged (over the period of precession about the magnetic line) cross section of a granule, as seen by an observer looking along the line of gas flow. To summarize, the average time between two sequent crossovers is proportional to an active site’s lifetime, the latter being proportional to the rate of gas-grain collisions, which in its turn is proportional to the effective cross section of the precessing granule in the flow. All in all, the dust particle will spend longer times in rotational states of smaller effective cross section. The cross section mechanism is essential for both rapid and slow flows.¹¹

This line of reasoning, developed by Lazarian, brings into play several timescales. One is the period t_{rot} of grain spin about its own rotation axis. The other is the wobble period t_{wobble} , i.e., the period of precession of the angular velocity Ω and major-inertia axis Z about the angular momentum J . Third is the period T of precession of J about the magnetic line B . The fourth one is the mean time τ between subsequent flip-overs of the granule.

Suprathermal rotation is swift: time t_{rot} is much shorter than the other timescales involved. Time t_{wobble} is irrelevant in the suprathermal case because in this case we neglect the wobble: as explained in § 1, the grain’s magnetic moment, the angular velocity vector, and the maximum-inertia axis are all aligned along the angular momentum, and they all precess about B , always remaining parallel to one another. The rate of this precession about B is slower than the granule’s rotation but still rapid enough: as mentioned in § 1, the precession period T is much shorter than a typical interval τ between crossovers. A crossover of a spinning particle can happen for one (or both) of two reasons: (1) spin damping through collisions with gas atoms and (2) grain resurfacing that alters positions of active sites. Without going into detailed dynamics, let us assume that on the average a cross-

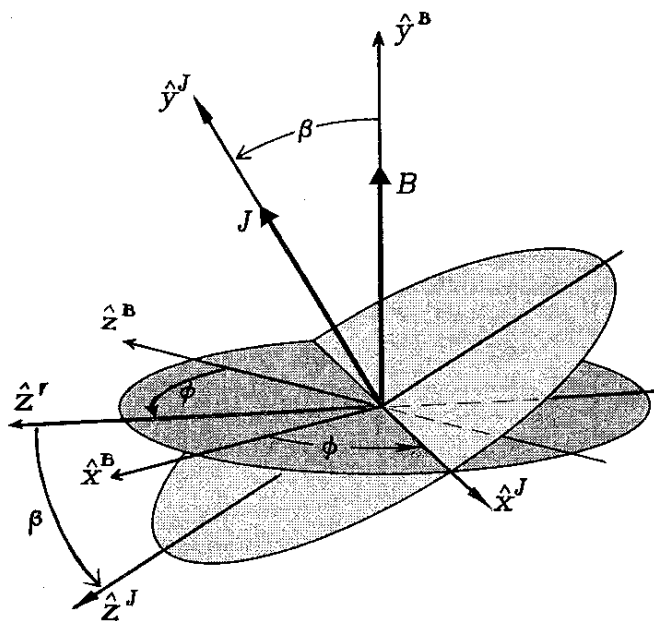


FIG. 2.—Relative positions of the coordinate systems associated with the magnetic line and with the angular momentum. The latter system is obtained from the former through a rotation about axis y^B , by angle ϕ , and a subsequent rotation about axis x^J , by angle β .

¹¹ For high ($>2 \text{ km s}^{-1}$) relative velocities, the cross section mechanism coerces the grain to align in the same direction as the crossover mechanism does (Lazarian 1995b). For slower flows, the stochastic torques produced by the Purcell rockets exceed the torques caused by collisions with gas. Thence, no considerable alignment will arise during the flip-overs. This makes the role of the crossover mechanism marginal. Therefore, one may expect that the cross section mechanism will dominate in slow flows. Still, the flow should be, at least, mildly supersonic, in order for the drift to dominate over the stochastic motion of individual atoms.

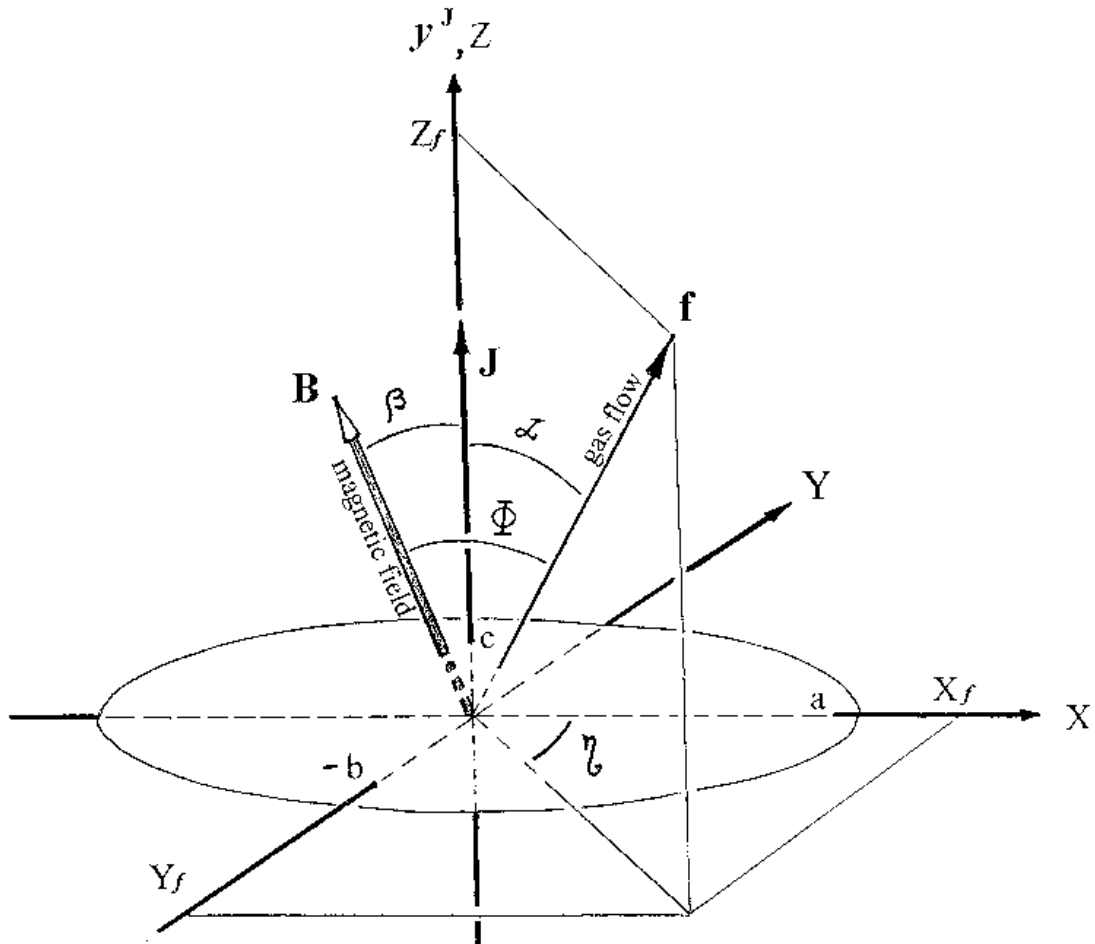


FIG. 3.—Relative orientation of the gas flow (depicted by vector f), principal axes of the ellipsoidal granule, and its angular momentum J . In the principal rotation state the major-inertia axis Z of the body (which is its shortest dimension) is aligned with J .

over takes place after the granule experiences N collisions. Suppose that this number of collisions is achieved during time τ :

$$N = \int_0^\tau nu \langle S \rangle_\eta dt, \tag{11}$$

n being the density of atoms, u being the speed of gas flow, and $\langle S \rangle_\eta$ being the cross section of the gas-grain interaction, averaged over the grain's (principal) rotation about J ,

$$\langle S \rangle_\eta = \frac{1}{2\pi} \int_0^{2\pi} S(\Phi, \beta, \phi, \eta) d\eta, \tag{12}$$

with angles Φ , β , ϕ , and η as in Figures 2 and 3. After averaging, $\langle S \rangle$ still remains time dependent, as a result of the precession of J about B . For times τ much longer than the precession period T ,

$$N = \frac{\tau}{T} \int_0^T nu \langle S \rangle_\eta dt, \tag{13}$$

whence

$$\tau = \frac{N}{nu(1/T) \int_0^T \langle S \rangle_\eta dt}. \tag{14}$$

It can be also rewritten as

$$\tau = \frac{N}{nu(1/2\pi) \int_0^{2\pi} \langle S \rangle_\eta d\phi} = \frac{N}{nu(1/2\pi) \langle \langle S \rangle_\eta \rangle_\phi}, \tag{15}$$

ϕ being the angle as in Figure 2; during a precession cycle it changes from 0 to 2π . The probability to find a granule in a certain spin state is proportional to the time it stays there. After averaging over the rotation about J , and after a further averaging over the precession, the so-averaged spin state depends on two arguments: the precession cone half-angle β and the angle Φ between the magnetic line and gas drift (Fig. 3). Thence, what the above formula gives us is the (not yet normalized) distribution of the (doubly averaged) spin states over β (angle Φ being fixed and playing the role of parameter). What then remains is simply to normalize, i.e., to divide τ by its integrand over the solid angle. Thus, we come to distribution

$$p(\beta) = \frac{1}{C} \frac{1}{\langle \langle S \rangle_\eta \rangle_\phi}, \tag{16}$$

with the normalization constant equal to

$$C = \int_0^{2\pi} d\beta \sin \beta \frac{1}{\langle \langle S \rangle_\eta \rangle_\phi} \tag{17}$$

and the average defined as

$$\langle\langle S \rangle\rangle_\phi = \int_0^{2\pi} d\phi \int_0^{2\pi} d\eta S. \tag{18}$$

This distribution being on our hands, the Rayleigh reduction factor is straightforward:

$$R = \frac{3}{2} \left(\langle \cos^2 \beta \rangle - \frac{1}{3} \right) = \frac{3}{2} \left[\int_0^{2\pi} d\beta \sin \beta p(\beta) \cos^2 \beta - \frac{1}{3} \right]. \tag{19}$$

This is where the physics ends and mathematics begins.

5. THE DISTRIBUTION OF β FOR TRIAXIAL ELLIPSOID-SHAPED GRAINS

To make the section readable, we shall move the calculations to Appendices B and C. Beside geometry, these include elements of the variational calculus, a heavy-duty tool seldom required in astrophysics.

Distribution $p(\beta)$ depends on angle Ψ between the magnetic line and the gas flow and on the geometry of grain (assuming that all particles in the cloud are alike). We shall model the cosmic-dust particle with an ellipsoid of semiaxes $a \geq b \geq c$ implementing body frame (X, Y, Z) . As we know from § 1, in the suprathermal case the major-inertia axis and the angular velocity are aligned with the angular momentum \mathbf{J} . Thus, vector \mathbf{J} is pointing along Z . Another frame, (x_B, y_B, z_B) , will be associated with the magnetic field \mathbf{B} , axis y_B pointing along \mathbf{B} (Fig. 2). The direction of gas flow will be denoted by unit vector \mathbf{f} with components (X_f, Y_f, Z_f) in the body frame. The angle between \mathbf{f} and axis Z will be called α (Fig. 3). The third coordinate system needed, (x_J, y_J, z_J) , will be associated with the angular momentum vector so that y_J will be parallel to \mathbf{J} and, therefore, to Z . Then axes x_J and z_J will belong to plane (X, Y) . One is free to parameterize the rapid rotation of the granule about its major-inertia axis Z by angle η between the least-inertia axis X and the gas flow projection on the plane (X, Y) . The suprathermal spin about \mathbf{J} is a much faster process than the precession of \mathbf{J} about the magnetic line. Therefore, while averaging over η , one may assume the orientation of \mathbf{J} being unaltered. This means that during several rotations of the granule (about \mathbf{J}) the angle α between \mathbf{J} and the gas flow may be assumed unchanged. We shall also need angle Φ between the gas flow and the magnetic field, and angle β between the magnetic field and the angular momentum. Finally, we shall parameterize the precession of \mathbf{J} about \mathbf{B} by angle ϕ (Fig. 2). This angle is constituted by axis z_B and axis z' (which is the projection of \mathbf{J} on the plane perpendicular to \mathbf{B}). Without loss of generality, one can direct axis x_B along the gas-flow projection on the plane perpendicular to \mathbf{B} .

As evident from Figure 4, angles $\alpha, \beta, \Phi,$ and ϕ are not all independent. They obey the (proven in Appendix B) relation

$$\cos \alpha = \cos \Phi \cos \beta + \sin \Phi \sin \beta \sin \phi. \tag{20}$$

The gas flow speeding by the ellipsoid defines an elliptic curve bounding area Σ hatched on Figure 5 and depicted by

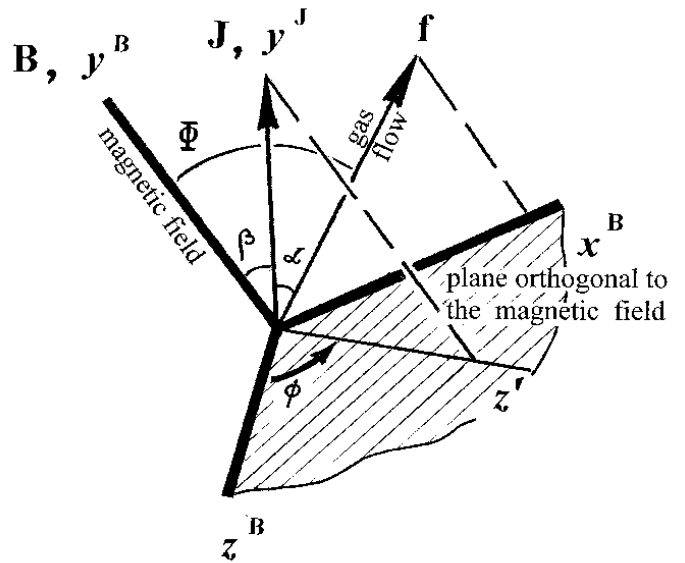


FIG. 4.—Axis y^B is chosen to point along the magnetic line. Axis x^B is chosen to point along the projection of the flow on the plane orthogonal to magnetic field \mathbf{B} . Auxiliary axis z' points along the projection of the angular momentum \mathbf{J} on the said plane.

a thick solid line on Figure 6. Evidently,

$$\Sigma = \pi |\rho_{\min} \times \rho_{\max}| = \pi \rho_{\min} \rho_{\max}, \tag{21}$$

ρ_{\min} and ρ_{\max} being the semiaxes of hatched ellipse. Projection of Σ on the plane orthogonal to the gas flow will give us the cross section S of the granule as seen by the observer looking at it along the line of wind. As shown in Appendix B,

$$S = \pi |n_x \cos \eta \sin \alpha + n_y \sin \eta \sin \alpha + n_z \cos \alpha|, \tag{22}$$

where the body-frame components of the auxiliary vector $\mathbf{n} \equiv \rho_{\min} \times \rho_{\max}$ are expressed by

$$n_x = (\rho_{\min})_y (\rho_{\max})_z - (\rho_{\min})_z (\rho_{\max})_y \tag{23}$$

and its cyclic transpositions. The components of ρ_{\min} and

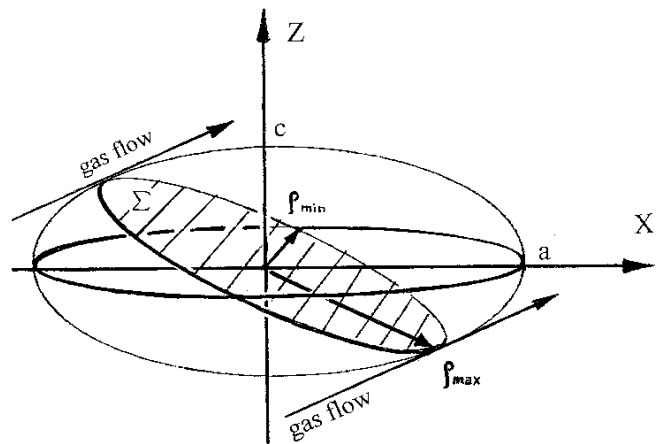


FIG. 5.—Gas flow passing by a granule tangential to its surface in certain points. Altogether such points constitute an ellipse whose interior is hatched. Its semiaxes are vectors ρ_{\min} and ρ_{\max} .

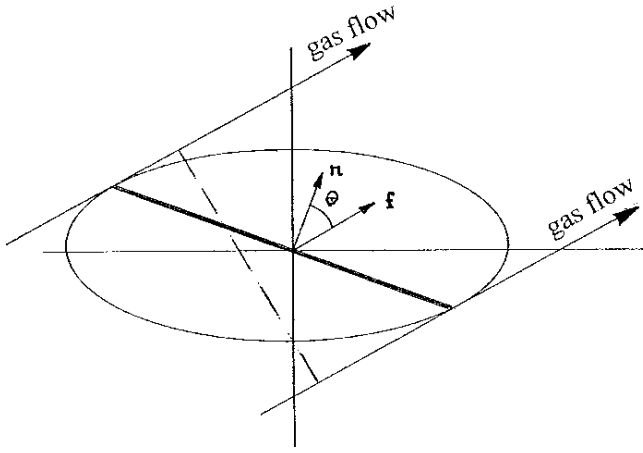


FIG. 6.—Granule in the gas flow. The thick solid line denotes cross section Σ (the one that is hatched on Fig. 5). The dashed line is the cross section S of the granule relative to the flow. Unit normals to these cross sections, \mathbf{n} and \mathbf{f} , are separated by angle θ .

ρ_{\max} depend on the lengths a , b , c of the semiaxes and on their orientation relative to the gas flow, i.e., on angles η and α . Angle α , in its turn, depends on β , Φ , and ϕ . All this will, eventually, enable us to express S via a , b , c , β , Φ , ϕ , and η . After that we shall average over η (i.e., over the principal rotation about \mathbf{J}) and over ϕ (i.e., over the precession of \mathbf{J} about \mathbf{B}). It will give us the distribution of equation (16) over β , bearing dependence also on a , b , c , and Φ as parameters.

Calculation of components of vector \mathbf{n} is presented in Appendix C. Plugging these into equation (22) entails the following expression for the cross section of the grain placed in the flow:

$$S = \frac{\pi}{4} \mu_1 \mu_2 |\sin^2 \alpha \cos \alpha \sin \eta \cos \eta| \left[\frac{1}{(b^2 - \lambda_2)(c^2 - \lambda_1)} - \frac{1}{(c^2 - \lambda_2)(b^2 - \lambda_1)} + \frac{1}{(c^2 - \lambda_2)(a^2 - \lambda_1)} - \frac{1}{(a^2 - \lambda_2)(c^2 - \lambda_1)} + \frac{1}{(a^2 - \lambda_2)(b^2 - \lambda_1)} - \frac{1}{(b^2 - \lambda_2)(a^2 - \lambda_1)} \right], \quad (24)$$

where

$$\mu_1 = 2 \left\{ \left[\frac{\sin \alpha \cos \eta}{a(a^2 - \lambda_1)} \right]^2 + \left[\frac{\sin \alpha \sin \eta}{b(b^2 - \lambda_1)} \right]^2 + \left[\frac{\cos \alpha}{c(c^2 - \lambda_1)} \right]^2 \right\}^{-1/2}, \quad (25)$$

$$\mu_2 = 2 \left\{ \left[\frac{\sin \alpha \cos \eta}{a(a^2 - \lambda_2)} \right]^2 + \left[\frac{\sin \alpha \sin \eta}{b(b^2 - \lambda_2)} \right]^2 + \left[\frac{\cos \alpha}{c(c^2 - \lambda_2)} \right]^2 \right\}^{-1/2}, \quad (26)$$

$$\lambda_{1,2} = \frac{-Q \pm \sqrt{Q^2 - 4PR}}{2P}, \quad (27)$$

$$P = \left(\frac{\sin \alpha \cos \eta}{a} \right)^2 + \left(\frac{\sin \alpha \sin \eta}{b} \right)^2 + \left(\frac{\cos \alpha}{c} \right)^2, \quad (28)$$

$$Q = - \left[\left(\frac{\sin \alpha \cos \eta}{a} \right)^2 (b^2 + c^2) + \left(\frac{\sin \alpha \sin \eta}{b} \right)^2 (c^2 + a^2) + \left(\frac{\cos \alpha}{c} \right)^2 (a^2 + b^2) \right], \quad (29)$$

$$R = \left(\frac{\sin \alpha \cos \eta}{a} \right)^2 b^2 c^2 + \left(\frac{\sin \alpha \sin \eta}{b} \right)^2 c^2 a^2 + \left(\frac{\cos \alpha}{c} \right)^2 a^2 b^2. \quad (30)$$

What remains is to average S over η and ϕ (using eq. [20]) and to plug the inverse of $\langle \langle S \rangle \rangle_{\eta, \phi}$ into equations (16)–(18) for distribution $p(\beta)$. The latter will give us, through equation (19), the Rayleigh reduction factor as a function of the granule dimensions a , b , and c and of the angle Φ between the magnetic field and the gas drift. This work can be performed only numerically and must be carried out with great care. The difficulty emerges from the fact that the denominators of the terms in square brackets in equation (24) for S vanish at certain values of the angles and at certain values of a , b , and c . Fortunately, this is fully compensated by the multipliers $\mu_1 \mu_2 |\sin^2 \alpha \cos \alpha \sin \eta \cos \eta|$ (which is most natural, for the area of a shadow cast by a smooth granule cannot have singularities). Still, when it comes to numerics, the mentioned issue demands much attention.

6. RESULTS AND THEIR PHYSICAL INTERPRETATION

The results of computation are presented in Figures 7–9. As expected, the diagrams in all three figures show the symmetry that corresponds to the invariance under inversion of the magnetic field direction. For another easy checkup, we see that on all the diagrams the Rayleigh reduction factor vanishes in the limit of spherical grains.

We see that the cross section Lazarian alignment is intensive for oblate granules (Fig. 7) and approaches its maximum in the limit of “flat flake” shape. The alignment is maximal when the flow is parallel (or antiparallel) to the magnetic line or is perpendicular thereto. Between these extremes, the alignment goes through zero. To explain this, let us consider the simple case of flat flake, and recall that the granule, roughly speaking, “wants” to minimize its (averaged over rotation and precession) cross section as “seen” by the flow. When the flow is parallel (or antiparallel) to the magnetic line about which the grain precesses, the average cross section is minimal if the flake has its precession cone half-angle β close to $\pi/2$ (and its square cosine close to nil). The R factor will be negative. When the drift is orthogonal to the magnetic field, the flake “prefers” to minimize its average cross section by rotating at β close to zero (with its squared cosine close to unity). The R factor will be positive.¹² Therefore, R passes through zero when

¹² Analytical treatment is possible in the cases of $\Phi = 0$ (when radiation-pushed grains follow the magnetic line) and $\Phi = \pi/2$ (when the grains are subject to Alfvénic waves or ambipolar diffusion). For details see Lazarian & Efrimov (1996).

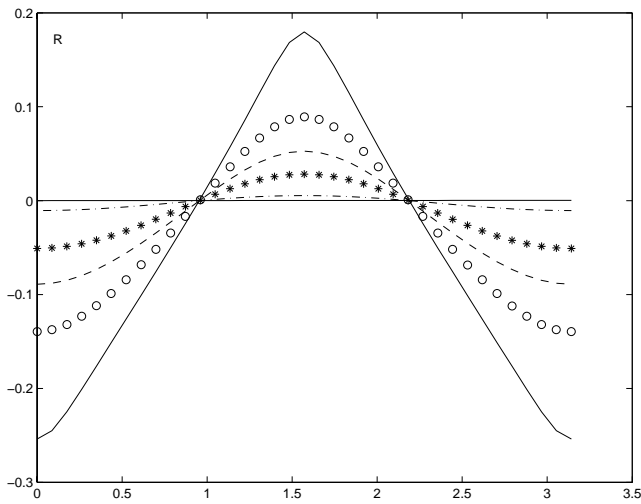


FIG. 7.—Rayleigh reduction factor R as a function of the angle Φ between the magnetic field and the gas flow, for the case of oblate symmetrical granules (“flakes”). The solid line corresponds to the semiaxes’ ratio $1 : 1 : 1/10$, the circle line corresponds to $1 : 1 : \frac{1}{3}$, the dashed line corresponds to $1 : 1 : \frac{1}{2}$, the asterisk line corresponds to $1 : 1 : \frac{2}{3}$, and the dot-dashed line corresponds to $1 : 1 : 0.9$.

the angle takes some intermediate value, which may be different for different ratios of semiaxes. Contrary to the expectations, however, this value, Φ_0^{oblate} , bears no dependence on the semiaxes’ ratio.

As evident from Figure 8, the effect is much weaker in the case of prolate grains.¹³ The diagrams are similar to those of the oblate case, and the physical interpretation is the same as above. Just as in the case of oblate geometry, the R factor goes through zero at some value of Φ , which may depend on

¹³ This case was studied in Lazarian et al. (1996). Our Fig. 8 is in full agreement with Fig. 3 from that paper. Mind, however, that in Fig. 3 in the said paper there is a slip of the pen: in fact, Φ was changing not from 0 through $\pi/2$ but from $\pi/2$ through π .

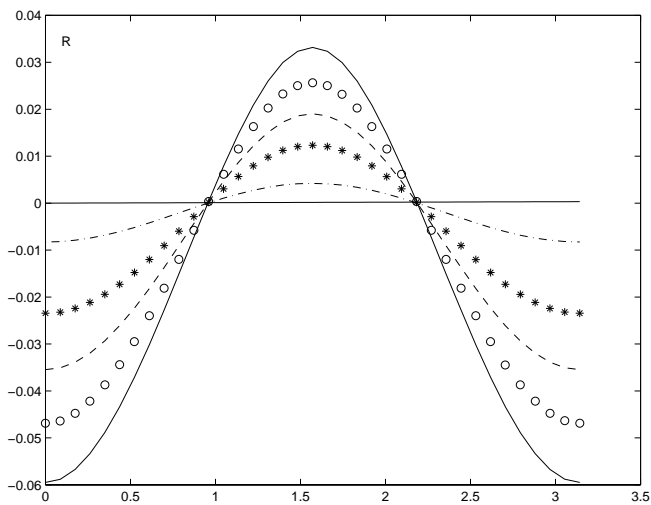


FIG. 8.—Same as Fig. 7, but for the case of prolate symmetrical granules (“rods”). The solid line corresponds to the semiaxes’ ratio $1 : 1/10 : 1/10$, the circle line corresponds to $1 : \frac{1}{3} : \frac{1}{3}$, the dashed line corresponds to $1 : \frac{1}{2} : \frac{1}{2}$, the asterisk line corresponds to $1 : \frac{2}{3} : \frac{2}{3}$, and the dot-dashed line corresponds to $1 : 0.9 : 0.9$.

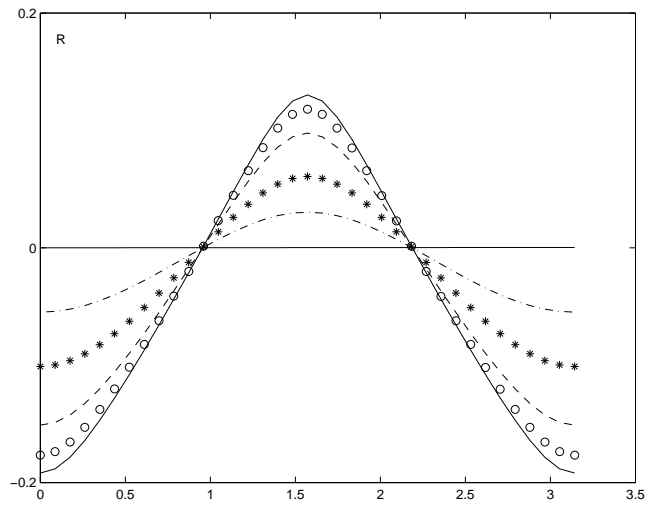


FIG. 9.—Same as Fig. 7, but for the case of triaxial asymmetrical granules. The solid line corresponds to the semiaxes ratio $1 : 0.9 : 0.2$, the circle line corresponds to $1 : 0.7 : 0.2$, the dashed line corresponds to $1 : 0.5 : 0.2$, the asterisk line corresponds to $1 : 0.3 : 0.2$, and the dot-dashed line corresponds to $1 : 0.2 : 0.2$.

the semiaxes’ ratio. Remarkably, in this case, too, such a dependence is absent, and all the curves cross the horizontal axis in the same point Φ_0^{prolate}

Moreover, the angles Φ_0^{prolate} seem to coincide with Φ_0^{oblate} and (within the limits imposed by the calculation error) equal $\arccos(1/\sqrt{3})$. Such miraculous coincidence must reflect some physical circumstances that are not evident at first glance. A straightforward analytic proof of this “coincidence,” even in the simplest, oblate case, is unavailable.

The third picture, Figure 9, accounts for the general case of a triaxial body, never addressed in the literature hitherto. Since the triaxial case is somewhat in between the oblate and prolate cases, it is not surprising that the diagrams have similar form. What is surprising is that once again all the curves seem to pass zero in the same point, $\Phi_0 = \arccos(1/\sqrt{3})$ [and, for symmetry reasons, in $\Phi_0 = \pi - \arccos(1/\sqrt{3})$]. Interestingly, the Gold alignment of thermal dust fails at the same values of Φ (Dolginov & Mytrofanov 1976). This maddening coincidence makes us suppose that this special value, $\Phi_0 = \arccos(1/\sqrt{3})$, is completely shape invariant and is independent from the suprathermality degree. Hence, here comes “the $\arccos(1/\sqrt{3})$ hypothesis”: no mechanical alignment of arbitrarily shaped (not necessarily ellipsoidal) thermal or suprathermal grains takes place, when the magnetic line and the gas drift make angle $\arccos(1/\sqrt{3})$ or $\pi - \arccos(1/\sqrt{3})$.

7. CONCLUSIONS

In the article thus far, we have investigated the cross section mechanism of suprathermal grain alignment in a supersonic interstellar gas stream. While the preceding efforts had been aimed at the cases of oblate and prolate ellipsoidal grains, in the current paper we studied the case of triaxial ellipsoid. We provided a comprehensive semianalytical, seminumerical treatment that reveals the dependence of the alignment measure (Rayleigh reduction factor R) on the semiaxes’ ratios and on the angle Φ between the magnetic line and gas drift. We provided a qualitative physical explanation of some of the obtained results.

However, the most intriguing result poses a puzzle and still lacks a simple physical explanation. This is the remarkable shape independence of the critical value of Φ , at which R vanishes and the cross section mechanism fails. For all

studied shapes (prolate, oblate, and triaxial with various ratios of semi-axes), this critical value is $\Phi_o = \arccos(1/\sqrt{3})$. We hypothesize that this special nature of the said value of Φ is shape independent.

APPENDIX A

RELATIONS BETWEEN THE OBSERVER-FRAME AND BODY-FRAME EXTINCTION CROSS SECTIONS

Our goal is to compute the extinction cross sections C_x^o and C_y^o for the two linear polarizations orthogonal to one another and to the line of sight, z_o . These so-called observer-frame cross sections should be expressed through extinction cross sections C_X, C_Y, C_Z appropriate to polarizations along the principal axes X, Y, Z of the granule (with X, Y , and Z standing for the minimal-, middle-, and maximal-inertia axes, respectively).

As an intermediate step, let us first calculate the intensities E_x^{o2} and E_y^{o2} appropriate to the linear polarizations x_o and y_o . These observer-frame intensities should be expressed through the body-frame intensities E_X^2, E_Y^2, E_Z^2 appropriate to polarizations along the principal axes. To that end, one has to perform a sequence of coordinate transformations.

The first step is to express E_x^o and E_y^o through the components $E_{x,y,z}^B$ of \mathbf{E} in the coordinate system associated with the magnetic line. In the observer's frame, axis z_o points toward the telescope, while y_o may be chosen to belong to the plane defined by z_o and \mathbf{B} . Then the magnetic line will lay in the (y_o, z_o) -plane. A coordinate system associated with the magnetic field (Fig. 1) may be defined with y_B pointing along \mathbf{B} and with the x -axis remaining untouched: $x_B = x_o$. The angle between \mathbf{B} and y_o (equal to that between z_B and z_o) will be called γ . Hence,

$$E_x^o = E_x^B, \quad E_y^o = E_y^B \cos \gamma + E_z^B \sin \gamma. \quad (\text{A1})$$

The next transformation is from (x_B, y_B, z_B) to (x_J, y_J, z_J) , the latter frame being affiliated to the (precessing about \mathbf{B}) angular momentum \mathbf{J} of the grain. We choose y_J to point along \mathbf{J} , at the angular separation β from y_B (Fig. 2). Vector \mathbf{J} describes, about \mathbf{B} , a precession cone of half-angle β , and so does y_J about y_B . An instantaneous position of the rotating frame (x_J, y_J, z_J) , with respect to the inertial one, (x_B, y_B, z_B) , is determined by angle ϕ . We see that a transition from (x_B, y_B, z_B) is composed of two steps. First, we must revolve the basis about the y_B axis by ϕ . This will map axes x_B and z_B onto axes x_J and z' , accordingly. Then we rotate the basis about x_J by angle β . In the course of a precession cycle of \mathbf{J} about \mathbf{B} , angle β remains unaltered, while ϕ describes the full circle. The relations between the unit vectors are straightforward:

$$\hat{\mathbf{z}}' = \hat{\mathbf{z}}^B \cos \phi - \hat{\mathbf{x}}^B \sin \phi, \quad (\text{A2})$$

$$\hat{\mathbf{z}}^J = \hat{\mathbf{z}}' \cos \beta - \hat{\mathbf{y}}^B \sin \beta = \hat{\mathbf{z}}^B \cos \phi \cos \beta - \hat{\mathbf{x}}^B \sin \phi \cos \beta - \hat{\mathbf{y}}^B \sin \beta, \quad (\text{A3})$$

$$\hat{\mathbf{y}}^J = \hat{\mathbf{y}}^B \cos \beta + \hat{\mathbf{z}}' \sin \beta = \hat{\mathbf{y}}^B \cos \beta + \hat{\mathbf{z}}^B \cos \phi \sin \beta - \hat{\mathbf{x}}^B \sin \phi \sin \beta, \quad (\text{A4})$$

$$\hat{\mathbf{x}}^J = \hat{\mathbf{x}}^B \cos \phi + \hat{\mathbf{z}}^B \sin \phi. \quad (\text{A5})$$

Plugging thereof into the right-hand side of the trivial identity $E_x^B \hat{\mathbf{x}}^B + E_y^B \hat{\mathbf{y}}^B + E_z^B \hat{\mathbf{z}}^B = \mathbf{E} = E_x^J \hat{\mathbf{x}}^J + E_y^J \hat{\mathbf{y}}^J + E_z^J \hat{\mathbf{z}}^J$ yields

$$E_x^B = E_x^J \cos \phi - E_y^J \sin \phi \sin \beta - E_z^J \sin \phi \cos \beta, \quad (\text{A6})$$

$$E_y^B = E_y^J \cos \beta - E_z^J \sin \beta, \quad (\text{A7})$$

$$E_z^B = E_x^J \sin \phi + E_y^J \cos \phi \sin \beta + E_z^J \cos \phi \cos \beta. \quad (\text{A8})$$

Lastly, we take into account the position of the grain itself, relative to frame (x^J, y^J, z^J) . As explained in footnote 1, it is legitimate in the suprathreshold case to assume that the major-inertia axis Z of the particle is aligned with the angular momentum, i.e., with axis y^J (see Lazarian & Efrimsky 1999). Rotation of the granule is, thus, assumed principal and may be parameterized by the angle ψ between the least-inertia axis X and z^J (this angle is equal to that between the middle-inertia axis Y and x^J). This gives

$$E_x^J = -E_X \sin \psi + E_Y \cos \psi, \quad (\text{A9})$$

$$E_y^J = E_Z, \quad (\text{A10})$$

$$E_z^J = E_X \cos \psi + E_Y \sin \psi. \quad (\text{A11})$$

Combination of all the previously presented transformations results in

$$\begin{aligned} E_x^o &= E_x^B = E_x^J \cos \phi - E_y^J \sin \phi \sin \beta - E_z^J \sin \phi \cos \beta \\ &= E_X (-\sin \psi \cos \phi - \cos \psi \sin \phi \cos \beta) + E_Y (\cos \psi \cos \phi - \sin \psi \sin \phi \cos \beta) - E_Z \sin \phi \sin \beta \end{aligned} \quad (\text{A12})$$

and

$$\begin{aligned}
 E_y^o &= E_y^B \cos \gamma + E_z^B \sin \gamma \\
 &= (E_y^J \cos \beta - E_z^J \sin \beta) \cos \gamma + (E_x^J \sin \phi + E_y^J \cos \phi \sin \beta + E_z^J \cos \phi \cos \beta) \sin \gamma \\
 &= E_X(-\sin \psi \sin \gamma \sin \phi - \cos \psi \cos \gamma \sin \beta + \cos \psi \cos \phi \sin \gamma \cos \beta) \\
 &\quad + E_Y(\cos \psi \sin \gamma \sin \phi - \sin \psi \cos \gamma \sin \beta + \sin \psi \cos \phi \sin \gamma \cos \beta) \\
 &\quad + E_Z(\cos \gamma \cos \beta + \sin \gamma \cos \phi \sin \beta),
 \end{aligned}
 \tag{A13}$$

whence the intensities averaged over the ensemble read

$$\begin{aligned}
 \langle E_x^{o2} \rangle &= \frac{1}{4} E_X^2 (1 + \langle \cos^2 \beta \rangle) + \frac{1}{4} E_Y^2 (1 + \langle \cos^2 \beta \rangle) + \frac{1}{2} E_Z^2 \langle \sin^2 \beta \rangle \\
 &= \frac{1}{3} (E_X^2 + E_Y^2 + E_Z^2) + \frac{1}{3} \left[\frac{1}{2} (E_X^2 + E_Y^2) - E_Z^2 \right] \frac{3}{2} (\langle \cos^2 \beta \rangle - \frac{1}{3}) \\
 &= \frac{1}{3} (E_X^2 + E_Y^2 + E_Z^2) + \frac{1}{3} \left[\frac{1}{2} (E_X^2 + E_Y^2) - E_Z^2 \right] R,
 \end{aligned}
 \tag{A14}$$

$$\begin{aligned}
 \langle E_y^{o2} \rangle &= E_X^2 (\frac{1}{4} \sin^2 \gamma + \frac{1}{2} \cos^2 \gamma \langle \sin^2 \beta \rangle + \frac{1}{4} \sin^2 \gamma \langle \cos^2 \beta \rangle) + E_Y^2 (\frac{1}{4} \sin^2 \gamma + \frac{1}{2} \cos^2 \gamma \langle \sin^2 \beta \rangle + \frac{1}{4} \sin^2 \gamma \langle \cos^2 \beta \rangle) \\
 &\quad + E_Z^2 (\cos^2 \gamma \langle \cos^2 \beta \rangle + \frac{1}{2} \sin^2 \gamma \langle \sin^2 \beta \rangle) \\
 &= \frac{1}{3} (E_X^2 + E_Y^2 + E_Z^2) + (\frac{1}{3} - \cos^2 \gamma) \left[\frac{1}{2} (E_X^2 + E_Y^2) - E_Z^2 \right] \frac{3}{2} (\langle \cos^2 \beta \rangle - \frac{1}{3}) \\
 &= \frac{1}{3} (E_X^2 + E_Y^2 + E_Z^2) + (\frac{1}{3} - \cos^2 \gamma) \left[\frac{1}{2} (E_X^2 + E_Y^2) - E_Z^2 \right] R.
 \end{aligned}
 \tag{A15}$$

Following the established tradition, we single out the so-called Rayleigh reduction factor

$$R = \frac{3}{2} (\langle \cos^2 \beta \rangle - \frac{1}{3}).
 \tag{A16}$$

In equations (A14) and (A15) averaging over ψ and ϕ implies simply $(2\pi)^{-2} \int_0^{2\pi} d\psi \int_0^{2\pi} d\phi$, while the averaging over β remains so far unspecified; the appropriate distribution depends on the physics of gas-grain interaction and is calculated in § 4.

Now that we have expressed the observable intensities $\langle E_x^{o2} \rangle$ and $\langle E_y^{o2} \rangle$ via those appropriate to polarizations along the body axes, we can write down similar expressions interconnecting the extinction cross sections. Since the extinction is merely attenuation of power from the incident beam, the contributions to cross section from the body axes' directions will be proportional to the mean shares of power appropriate to these three axes:

$$C_x^o = \frac{C_X + C_Y + C_Z}{3} + \frac{1}{3} \left[\frac{1}{2} (C_X + C_Y) - C_Z \right] R
 \tag{A17}$$

and

$$C_y^o = \frac{C_X + C_Y + C_Z}{3} + \left(\frac{1}{3} - \cos^2 \gamma \right) \left[\frac{1}{2} (C_X + C_Y) - C_Z \right] R,
 \tag{A18}$$

wherefrom

$$C_x^o - C_y^o = \left[\frac{1}{2} (C_X + C_Y) - C_Z \right] R \cos^2 \gamma.
 \tag{A19}$$

APPENDIX B

ELLIPSOIDAL GRANULE PLACED IN A GAS FLOW

Let us calculate the angle α between the gas-flow direction \mathbf{f} and the maximum-inertia axis Z of the dust particle (Fig. 4). The dot product of the appropriate unit vectors

$$\hat{\mathbf{y}}_J = \hat{\mathbf{y}}_B \cos \beta + \hat{\mathbf{z}}_B \sin \beta \cos \phi + \hat{\mathbf{x}}_B \sin \beta \sin \phi
 \tag{B1}$$

and

$$\mathbf{f} = \hat{\mathbf{y}}_B \cos \Phi + \hat{\mathbf{z}}_B \sin \Phi
 \tag{B2}$$

leads to the formula

$$\cos \alpha = \cos \Phi \cos \beta + \sin \Phi \sin \beta \sin \phi.
 \tag{B3}$$

Another important relation is evident from Figure 3:

$$\cos \alpha = \frac{Z_f}{\sqrt{X_f^2 + Y_f^2 + Z_f^2}} . \quad (\text{B4})$$

In Figure 3, the projection of \mathbf{f} on (X, Y) will make an angle η with axis X , such that

$$\cos \eta \sin \alpha = \frac{X_f}{\sqrt{X_f^2 + Y_f^2 + Z_f^2}} , \quad \sin \eta \sin \alpha = \frac{Y_f}{\sqrt{X_f^2 + Y_f^2 + Z_f^2}} . \quad (\text{B5})$$

Equations (B4) and (B5) will enable us to calculate the grain's cross section relative to the wind. The lines of gas flow, which are tangential to the ellipsoid surface, touch this surface in points that altogether constitute a curve. It is the ellipse hatched on Figure 5. Its area is

$$\Sigma = \pi |\boldsymbol{\rho}_{\min} \times \boldsymbol{\rho}_{\max}| = \pi \rho_{\min} \rho_{\max} , \quad (\text{B6})$$

$\boldsymbol{\rho}_{\min}$ and $\boldsymbol{\rho}_{\max}$ being its semiaxes. Projection of Σ toward the plane perpendicular to the gas flow is the cross section S of the granule, as seen by the observer looking at it along the line of wind (Fig. 6). In other words, S is the "shadow" that the granule casts. Evidently,

$$S = |\cos \theta| \Sigma , \quad (\text{B7})$$

θ being the angle between the vector \mathbf{f} of the gas flow and vector

$$\mathbf{n} \equiv \boldsymbol{\rho}_{\min} \times \boldsymbol{\rho}_{\max} \quad (\text{B8})$$

orthogonal to the hatched ellipse. As follows from equations (B4) and (B5),

$$\begin{aligned} |\cos \theta| &= \frac{\mathbf{n} \cdot \mathbf{f}}{|\mathbf{n}| |\mathbf{f}|} = \frac{|n_x X_f + n_y Y_f + n_z Z_f|}{(\Sigma/\pi) \sqrt{X_f^2 + Y_f^2 + Z_f^2}} \\ &= \frac{\pi}{\Sigma} |n_x \cos \eta \sin \alpha + n_y \sin \eta \sin \alpha + n_z \cos \alpha| . \end{aligned} \quad (\text{B9})$$

Combining the above with equation (B7), we arrive at

$$S = \pi |n_x \cos \eta \sin \alpha + n_y \sin \eta \sin \alpha + n_z \cos \alpha| . \quad (\text{B10})$$

APPENDIX C

CROSS SECTION OF A GRANULE IN GAS STREAM

Every point (X, Y, Z) belonging to the surface of the ellipsoidal grain obeys the equation

$$g(X, Y, Z; a, b, c) \equiv \frac{X^2}{a^2} + \frac{Y^2}{b^2} + \frac{Z^2}{c^2} = 1 . \quad (\text{C1})$$

The points that constitute the boundary of the hatched figure Σ on Figure 5 obey equation (C1), along with one more relation. That second one is the condition of flow being tangential to the surface in these points. Stated alternatively, a normal to the ellipsoid in point (X, Y, Z) is given by vector $(X/a^2, Y/b^2, Z/c^2)$, and the flow must be orthogonal to this normal:

$$h(X, Y, Z; X_f, Y_f, Z_f) \equiv \frac{X X_f}{a^2} + \frac{Y Y_f}{b^2} + \frac{Z Z_f}{c^2} = 0 . \quad (\text{C2})$$

To find vectors $\boldsymbol{\rho}_{\min}$ and $\boldsymbol{\rho}_{\max}$ pointing from the center to the closest and the farthest points of the ellipse Σ , one has to employ the variational method:

$$\frac{\partial}{\partial X, Y, Z} (l^2 - \lambda g - \mu h) = 0 , \quad (\text{C3})$$

where $l^2 \equiv X^2 + Y^2 + Z^2$ and λ, μ are Lagrange multipliers. The latter equation gives us the values of X, Y, Z appropriate to the extremal distances from the origin, assuming that equations (C1) and (C2) hold. The three equations given by equation (C3), for X, Y , and Z , yield

$$X = \frac{\mu X_f}{2(a^2 - \lambda)} , \quad Y = \frac{\mu Y_f}{2(b^2 - \lambda)} , \quad Z = \frac{\mu Z_f}{2(c^2 - \lambda)} \quad (\text{C4})$$

for the extremal points where vectors $\pm \rho_{\min}$ and $\pm \rho_{\max}$ end. Now plug equation (C4) into equation (C2):

$$h = \mu \frac{X_f^2}{2a^2(a^2 - \lambda)} + \mu \frac{Y_f^2}{2b^2(b^2 - \lambda)} + \mu \frac{Z_f^2}{2c^2(c^2 - \lambda)} = 0. \tag{C5}$$

This entails

$$\lambda_{1,2} = \frac{-Q \pm \sqrt{Q^2 - 4PR}}{2P}, \tag{C6}$$

where

$$P \equiv \left(\frac{X_f}{a}\right)^2 + \left(\frac{Y_f}{b}\right)^2 + \left(\frac{Z_f}{c}\right)^2, \tag{C7}$$

$$Q \equiv -\left[\left(\frac{X_f}{a}\right)^2(b^2 + c^2) + \left(\frac{Y_f}{b}\right)^2(c^2 + a^2) + \left(\frac{Z_f}{c}\right)^2(a^2 + b^2)\right], \tag{C8}$$

$$R \equiv \left(\frac{X_f}{a}\right)^2 b^2 c^2 + \left(\frac{Y_f}{b}\right)^2 c^2 a^2 + \left(\frac{Z_f}{c}\right)^2 a^2 b^2. \tag{C9}$$

Substitution of equation (C4) into equation (C1) will lead to the expression for μ :

$$\mu^2 = 4 \left\{ \left[\frac{X_f}{a(a^2 - \lambda)} \right]^2 + \left[\frac{Y_f}{b(b^2 - \lambda)} \right]^2 + \left[\frac{Z_f}{c(c^2 - \lambda)} \right]^2 \right\}^{-1}. \tag{C10}$$

Since we have two acceptable values for λ , we shall obtain four different values for μ :

$$\mu_1 = 2 \left\{ \left[\frac{X_f}{a(a^2 - \lambda_1)} \right]^2 + \left[\frac{Y_f}{b(b^2 - \lambda_1)} \right]^2 + \left[\frac{Z_f}{c(c^2 - \lambda_1)} \right]^2 \right\}^{-1/2}, \tag{C11}$$

$$\mu_2 = 2 \left\{ \left[\frac{X_f}{a(a^2 - \lambda_2)} \right]^2 + \left[\frac{Y_f}{b(b^2 - \lambda_2)} \right]^2 + \left[\frac{Z_f}{c(c^2 - \lambda_2)} \right]^2 \right\}^{-1/2}, \tag{C12}$$

and $\mu_3 = -\mu_1$, $\mu_4 = -\mu_2$. Simply from looking at how λ and μ enter equation (C4) for extremal-point coordinates, we see that a change of sign of μ (with λ fixed) corresponds merely to a switch from ρ_{\min} (or ρ_{\max}) to $-\rho_{\min}$ (or $-\rho_{\max}$). Since it is irrelevant, for our purposes, which of the two opposite farthest from the origin points to call ρ_{\max} and which to call $-\rho_{\max}$ (and, similarly, which of the two closest to the origin points to call ρ_{\min} and which to call $-\rho_{\min}$), we shall take the positive values of μ only. As a result, a substitution of λ_1 and μ_1 into equation (C4) will give us the coordinates of one of the two farthest (from the center) points of the boundary of the hatched ellipse Σ . Similarly, plugging in λ_2 and μ_2 will provide us with the coordinates of one of the two closest points. The chosen farthest and closest points will have coordinates $(\rho_{\max})_{x,y,z}$ and $(\rho_{\min})_{x,y,z}$, respectively:

$$(\rho_{\max})_x = \frac{\mu_1 X_f}{2(a^2 - \lambda_1)}, \quad (\rho_{\max})_y = \frac{\mu_1 Y_f}{2(b^2 - \lambda_1)}, \quad (\rho_{\max})_z = \frac{\mu_1 Z_f}{2(c^2 - \lambda_1)}, \tag{C13}$$

$$(\rho_{\min})_x = \frac{\mu_2 X_f}{2(a^2 - \lambda_2)}, \quad (\rho_{\min})_y = \frac{\mu_2 Y_f}{2(b^2 - \lambda_2)}, \quad (\rho_{\min})_z = \frac{\mu_2 Z_f}{2(c^2 - \lambda_2)}. \tag{C14}$$

Further substitution of these expressions into equation (23) and into its cyclic transpositions will lead to

$$n_x X_f = X_f Y_f Z_f \frac{\mu_1 \mu_2}{4} \left[\frac{1}{(b^2 - \lambda_2)(c^2 - \lambda_1)} - \frac{1}{(c^2 - \lambda_2)(b^2 - \lambda_1)} \right], \tag{C15}$$

$$n_y Y_f = X_f Y_f Z_f \frac{\mu_1 \mu_2}{4} \left[\frac{1}{(c^2 - \lambda_2)(a^2 - \lambda_1)} - \frac{1}{(a^2 - \lambda_2)(c^2 - \lambda_1)} \right], \tag{C16}$$

$$n_z Z_f = X_f Y_f Z_f \frac{\mu_1 \mu_2}{4} \left[\frac{1}{(a^2 - \lambda_2)(b^2 - \lambda_1)} - \frac{1}{(b^2 - \lambda_2)(a^2 - \lambda_1)} \right]. \tag{C17}$$

Thence, the cross section S of the grain, relative to the gas-flow direction, will read

$$S = \frac{\pi}{4} \mu_1 \mu_2 |X_f Y_f Z_f| \left[\frac{1}{(b^2 - \lambda_2)(c^2 - \lambda_1)} - \frac{1}{(c^2 - \lambda_2)(b^2 - \lambda_1)} + \frac{1}{(c^2 - \lambda_2)(a^2 - \lambda_1)} - \frac{1}{(a^2 - \lambda_2)(c^2 - \lambda_1)} + \frac{1}{(a^2 - \lambda_2)(b^2 - \lambda_1)} - \frac{1}{(b^2 - \lambda_2)(a^2 - \lambda_1)} \right], \quad (\text{C18})$$

where $\lambda_{1,2}$ and $\mu_{1,2}$ are functions of (X_f, Y_f, Z_f) , the latter being functions of angles η and α (while α , in its turn, depends on β, Φ , and ϕ). All in all, the “shadow” area S turns out to be a function of angles β, Φ, η , and ϕ .

REFERENCES

- Alpar, A., & Ögelman, H. 1987, *A&A*, 185, 196
 Bisnovatyi-Kogan, G. S., & Kahabka, P. 1993, *A&A*, 267, L43
 Davis, J., & Greenstein, J. L. 1951, *ApJ*, 114, 206
 Dolginov, A. Z., & Mitrofanov, I. G. 1976, *Ap&SS*, 43, 291
 Draine, B. T., & Lee, H.-M. 1984, *ApJ*, 285, 89
 Draine, B. T., & Weingartner, J. C. 1996, *ApJ*, 470, 551
 ———. 1997, *ApJ*, 480, 633
 Efroimsky, M. 2000, *J. Math. Phys.*, 41, 1854
 ———. 2001, *Planet. Space Sci.*, 49, 937
 ———. 2002, *Adv. Space Res.*, 29, 725
 Gold, T. 1952, *MNRAS*, 112, 215
 Greenberg, J. M. 1968, in *Nebulae and Interstellar Matter*, Vol. VII, ed. B. M. Middlehurst & L. H. Aller (Chicago: Univ. Chicago Press), pp. 221–364
 Hall, J. S. 1949, *Science*, 109, 166
 Hildebrand, R. H. 1988, *QJRAS*, 29, 327
 Hiltner, W. A. 1949, *ApJ*, 109, 471
 Jones, R. V., & Spitzer, L., Jr. 1967, *ApJ*, 147, 943
 ———. 1995a, *A&A*, 293, 859
 ———. 1995b, *ApJ*, 451, 660
 ———. 1995c, *ApJ*, 453, 229
 ———. 1995d, *MNRAS*, 274, 679
 Jones, R. V., & Spitzer, L., Jr. 1995e, *MNRAS*, 277, 1235
 Lazarian, A., & Efroimsky, M. 1996, *ApJ*, 466, 274
 ———. 1999, *MNRAS*, 303, 673
 Lazarian, A., Efroimsky, M., & Ozik, J. 1996, *ApJ*, 472, 240
 Lazarian, A., & Roberge, W. G. 1997, *ApJ*, 484, 230
 Lee, H. M., & Draine, B. T. 1985, *ApJ*, 290, 211
 Martin, P. G. 1971, *MNRAS*, 153, 279
 ———. 1974, *ApJ*, 187, 461
 Purcell, E. M. 1979, *ApJ*, 231, 404
 Purcell, E. M., & Spitzer, L., Jr. 1971, *ApJ*, 167, 31
 Roberge, W. G., DeGraff, T. A., & Flaherty, J. E. 1993, *ApJ*, 418, 287
 Roberge, W. G., & Lazarian, A. 1999, *MNRAS*, 305, 615
 Spitzer, L., & Tukey, J. W. 1951, *ApJ*, 114, 187
 Stairs, I. H., et al. 2000, *Nature*, 406, 484
 Stoner, E. C. 1934, *Magnetism and Matter* (London: Methuen Publ.)
 Trümper, J., Kahabka, P., Ögelman, H., Pietsch, W., & Voges, W. 1986, *ApJ*, 300, L63
 van de Hulst, H. C. 1957, *Light Scattering by Small Particles* (New York: Dover)
 Whittet, D. C. B. 1992, *Dust in the Galactic Environment* (Bristol: IOP Publ.)